Analyst

PAPER

View Article Online
View Journal

Cite this: DOI: 10.1039/d6an00072j

Monte Carlo-like peaks assignment using a time-resolved *in situ* NMR approach for complex reaction monitoring: a case study of the photodegradation of retinyl acetate

Farwa Khalid, †[a] Chunchesh Malangi Gajendramurthy, *†[a] Franz F. Westermair, [b] Lena Miler, [c] Ruth M. Gschwind, [b] Tomasz Ratajczyk [a] and Mateusz Urbańczyk *[a]

Received 22nd January 2026,
Accepted 18th April 2026

DOI: 10.1039/d6an00072j

rsc.li/analyst

Photoactive molecules are of central interest due to their roles in light–matter interaction and in biological systems, and their applications in technology and medicine. Many important photoactive molecules undergo photodegradation, which is a complex, multi-path process involving many molecular species. One compelling case of photodecomposition involves retinyl acetate, which is necessary for vision processes. Here, we demonstrate a comprehensive approach in which the informativity of NMR can be harnessed for the in-depth investigation of the way in which photodegradation proceeds *via* a combination of two approaches: the interleaved time-resolved non-uniform sampling and time-resolved diffusion NMR. Specifically, the mass evolution, which was estimated from the first approach, was compared with the mass calculated from the diffusion coefficient estimated from the second approach, and the correlation between them was identified, enabling NMR signal assignment. This comparison is used for the Monte Carlo-like assignment, in which a vast library of potential reactants is scanned to determine the proper assignment. The presented approach is general-purpose and can be easily implemented for the investigation of many important photodegradation processes.

Introduction

The interest in photoactive molecules is currently increasing. This is because photoactive molecules are currently being widely utilized in materials chemistry and medicine. For example, photoactive molecules are used for the construction of complex functional photoactive materials, and they are also used in medical phototherapy in the treatment of serious diseases, including cancers. One can provide even more compelling examples than the ones mentioned above, and their descriptions can be found in many review articles.[1–9] The interaction of light with molecules can lead to the molecules' conformational changes or decomposition. Insight into these processes is pivotal in the context of obtaining an in-depth understanding of photochemistry and its applications. The photodegradation process is a complex reaction that can occur *via* a variety of possible pathways.[10,11] Moreover, many of the photogenerated products can share similar chemical structures – including isomers – which makes the analysis of such a system a tremendous task, as most of the analytic tools used for reaction monitoring might have a problem distinguishing reactants. One of the most important such instances with a host of biochemically relevant functions, but which undergoes detrimental photodegradation, is Retinyl Acetate (RA), which is also known as vitamin A acetate. RA has crucial importance in the pharmaceutical industry as a main compound used to deliver retinol to human beings. This substance is necessary for proper vision, immune function,[12] skin health, and the regulation of hormones[13] and enzymes.

RA was first synthesized by Hoffmann-La Roche in 1947[14] and is now used in both human supplements and animal feed to support overall health. Retinoids (particularly RA), including both natural and synthetic forms, have shown the ability to inhibit mammary carcinogenesis.[15] Their conjugated double bond system forms an electron-dense region, making them highly reactive. The polyene chain in these compounds can also undergo *cis–trans* isomerization. RA, commonly used in food fortification[16,17] is particularly vulnerable to degradation due to its double bonds and ester group, which are affected by

[a]*Institute of Physical Chemistry, Polish Academy of Sciences, Kasprzaka 44/52, 01-224 Warsaw, Poland. E-mail: murbanczyk@ichf.edu.pl, chunchesh.mg@ichf.edu.pl*
[b]*Faculty of Chemistry and Pharmacy, University of Regensburg, Universitätsstraße 31, 93053 Regensburg, Germany*
[c]*Faculty of Physics, University of Warsaw, Pasteura 5, 02-093 Warsaw, Poland*
†Those authors contributed equally.

light (UV), heat, oxygen, and peroxides. These conditions can alter its structure and reduce its effectiveness. Vitamin A derivatives were among the first recognized for hormone-like activity in the skin, participating in regulated processes such as metabolism,[18] and systemic distribution. As a result, considerable research has focused on improving their stability for use in food, supplements, and pharmaceuticals, and potentially yieldable photo products, which can be harmful to humans.[19–25] Therefore, the photostability of retinyl-based molecules and the possible pathways of their photodegradation are of vital importance.

Previous studies on the photodegradation of RA indicate that sunlight-induced degradation occurs much faster than for retinol.[26] Upon exposure to UV light, it shows the maximum absorption at 325 nm. It undergoes isomerization, forming a mixture of *cis* and *trans* isomers, with the solvent polarity influencing the extent of isomerization.[26–29] The isomerization of RA and its degraded products, such as vitamin A ethyl ether, 4-ethoxy anhydro vitamin A, anhydroretinol (AR), and the homodimer of RA in ethanol[30,31] occurs through an ionic photodissociation mechanism *via* cationic intermediates. Techniques like laser flash photolysis and pulse radiolysis have been used to identify the retinyl cation formed from the photoreaction of RA, which produces many products, such as retinyl methyl ether, acetic acid, and methyl acetate, along with AR in methanol, hexane, and acetone.[32–37] AR formation has been reported from the photoirradiation of retinyl palmitate (RP) under exposure to UVA, UVB, and UVC radiation in methanol and ethanol. The resulting products were confirmed by high-performance liquid chromatography (HPLC) and mass spectrometry.[38–40] Photooxidation of retinyl acetate in benzene, with a trace of water, resulted in different products such as dihydroacetinidiolide, β-ionone, 2-hydroxy-2,6,6-trimethyl cyclohexanone, geronic acid, and desoxyxanthoxin.[41] Recently, the UV stability of RA has been improved with butylated hydroxytoluene (BHT) by scavenging the free radicals, and converting them into a stable compound when dissolved in ethanol. In this process, isopropyl alcohol is also used to prevent the formation of AR.[42] This clearly shows that the reaction is heavily dependent on the initial conditions and can follow either an ionic or a radical pathway, resulting in many possible products. It is worth mentioning that previous studies have relied on the analysis of the reaction *ex situ* using various analytical techniques.

In this work we have decided to utilize a powerful method for investigating reactions and elucidating mechanisms, which is Nuclear Magnetic Resonance (NMR). The method is widely used for the studies of countless reactions.[43–50] However, one has to understand its limitations. The primary consideration for a complex mixture analysis is resolution. Especially in the case of the conventional one-dimensional ^{1}H NMR spectrum, the peaks from different compounds may heavily overlap, especially due to the low chemical shift dispersion.

There are several solutions to this issue, starting from pure-shift experiments,[51] to the introduction of additional dimensions, like ^{13}C (*e.g.*, HSQC) or diffusion (DOSY experiments[52]). However, the solution comes with a cost: the long acquisition time, which makes the utilization of such experiments unfeasible for reaction monitoring. The solution to improve the temporal resolution in pure-shift methodology is to utilize the novel fast pulse sequences like SHARPER,[53] the use of non-uniform sampling,[54] or deep learning.[55,56] In the case of two-dimensional methods, the popular solution is to use Ultra-Fast (UF) variants of those experiments,[57–59] or the Time-Resolved Non-Uniform Sampling (TR-NUS) approach.[60–62]

The UF method introduced by Frydman[57,63] relies on the encoding of the indirect dimension spatially along the sample. This method allows the acquisition of 2D spectra in a single scan and is used extensively for reaction monitoring.[50,64,65] The method allows for spatial encoding of the indirect dimension as a frequency or so-called Laplace NMR (relaxation or diffusion).[58] However, the method for now is limited by the loss of sensitivity and possible rise of artifacts due to sample inhomogeneity.[66]

The Time-Resolved (TR) methodology was introduced by Mayzel *et al.*[61] as a variant of NUS for time-dependent processes, and similarly to UF was quickly utilized as a tool for reaction monitoring.[48,60,62,67,68] This method relies on the long NUS scheme that covers the entire reaction time. After the acquisition, the data is divided into overlapping NUS experiments that can be later processed. The concept can also be extended to the diffusion dimension.[69–71] The comparison of both methods can be found here.[72]

In 2022, we demonstrated the synergy of TR-NUS HSQC and Time-Resolved Diffusion (TR-D) NMR for the study of the photopolymerization of bis-anthracene derivatives.[73] The use of both methods acquired in an interleaved manner allows us to obtain the information from diffusion coefficients to correctly assign the peaks in the HSQC spectra and completely follow the reaction. This seminal work showed that the information about the average molecular mass evolution, derived from diffusion coefficients, only correlates with the evolution of mass calculated from the peaks of HSQC when the peak assignment is correct.

In the current work, we build upon the methodology introduced previously,[73] adapting it to a much more complex and biologically relevant system: the photodegradation of retinyl acetate. In such a system, the number of potential products and intermediates is significantly larger than in our previous investigation, and, as mentioned before, the studied reaction can follow multiple pathways depending on the initial conditions. To overcome this issue, we have introduced a new peak assignment strategy based on the Monte Carlo approach.

Experimental section

Sample preparation

We purchased crystalline solid Retinyl Acetate (RA) from Sigma-Aldrich (USA) and ethanol-d_6 (99%) from Eurisotop (France). To prepare the NMR sample, 50 mg (0.1524 mmol) of RA was dissolved in 0.8 mL of deuterated ethanol-d_6. After stir-

ring the mixture in a sonicator at room temperature for 20 minutes, we used a Pasteur pipette to transfer 550 μl of the solution into a 5 mm PhotoNMR tube (NewEra, USA).

UV illumination setup

The sample was illuminated using a 365 nm LED (M365FP1, Thorlabs, Inc.), at a current of 1200 mA with a T-Cube LED driver (LEDD1B, Thorlabs). The LED was coupled to a 1-meter FT400EMT multimode optical fiber (∅400 μm core, 0.39 NA, Thorlabs) and measured a maximum power output of 6.5 mW at the fiber end. For all experiments, the UV light was delivered through a 3-meter FT1000UMT multimode optical fiber (∅1000 μm core, 0.39 NA, Thorlabs) with a sandblasted tip, as reported previously.[74] The optical fiber was secured in a coaxial insert and placed in a PhotoNMR tube (NewEra USA). Controlled switching of the LED (illumination only during the ^{1}H NMR acquisition) was achieved with a modified script in TopSpin, which allowed control of an Arduino Uno. The Arduino was programmed to generate a PWM signal that could be used to set the illumination power to any value between 0% and 100%. The Arduino was connected to the LED driver with a BNC-cable. The desired illumination power was stored in the spectra in the constant arrays in CNST61 and sent to the Arduino at the beginning of each new measured spectrum. Initially, we set the illumination power to 0% for the first 4 hours of acquisition. At the 4-hour mark, we increased the power to 20% and maintained that level for 35 hours. Then, we raised the power to 40% and kept it constant until the 46th hour of the illumination.

NMR

We performed all NMR experiments on a Bruker AVANCE Neo 300 MHz spectrometer equipped with a BBI 300 MHz W1 5 mm z-gradient probe with a BVT-3000 temperature controller. The spectrometer was controlled *via* the TOPSPIN 4.3 program.

We based the acquisition protocol on the TReNDS[60] acquisition script, modified with the addition of TR-D acquisition after TR-NUS and control of illumination. The interval between consecutive HSQC, DOSY, or ^{1}H NMR experiments is 252s. The general scheme of the acquisition is presented in Fig. 1.

Time-resolved diffusion NMR. We have used the dstebpgp3s1d pulse sequence as a base for the acquisition of the TR-D experiment. The acquisition parameters for interleaved acquisition were as follows: Δ: 50 ms, δ: 2 ms, pulse length: 8.25 μs, relaxation delay 1 s, number of scans: 16. The pulsed-field gradient strength for all data sets was set as a shuffled linear spaced array of 32 values from 2.72 to 51.69 G cm^{-1} repeated for the entire acquisition length.

Time-resolved non-uniform sampling. We based the TR-NUS acquisition on the hsqcgpph pulse sequence. We used the following acquisition parameters: a relaxation delay of 1.5 s, 16 scans, an indirect dimension spectral width of 165 ppm centered at 75 ppm, and a maximum evolution was set to 256 points in the indirect dimension. We generated the sampling schedule using a sampling generator from the MDDNMR package.[75]

Mass spectrometry

We performed mass spectrometry analyses using a Synapt G2-S mass spectrometer (Waters) equipped with an atmospheric pressure chemical ionization (APCI) ion source and a quadrupole time-of-flight (QTOF) mass analyzer. We dissolved the sample in dichloromethane, diluted it with methanol, and injected it directly into the electrospray ion source. We used methanol as the solvent at a flow rate of 100 μL min^{-1}. We carried out the measurements in both positive and negative ion modes, with the time-of-flight analyzer operating at a resolving power of 30 000 FWHM. We calibrated the instrument externally using sodium formate in the mass range of m/z 50–1200. We generated a lock spray spectrum of leucine-enkephalin using the lock spray source and applied corrections to every spectrum. We used nitrogen as the desolvation and cone gas, setting their flow rates to 600 L h^{-1} and 100 L h^{-1}, respectively. We set the source temperature to 120 °C and the probe temperature to 550 °C. We adjusted the nebulizer gas pressure to 5.0 bar. We set the corona current to 13.0 μA and adjusted the sampling cone voltage and source offset to 40 V. We controlled the instrument and processed the recorded data using the MassLynx V4.2 software package (Waters).

Data processing and analysis

We extracted all three interleaved experiments—TR NUS HSQC, TR-D, and 1H—into separate folders, then processed and analyzed them individually. We performed further analysis using Python 3.13, TopSpin 4.3, and the Dynamics Center 2.8.6 environment. As needed, we used the following packages: nmrglue,[76] NumPy,[77] SciPy,[78] and Matplotlib.[79]

^{1}H NMR. We imported the 1H spectra using nmrglue, and processed them with exponential apodization of 0.3 Hz and zerofilling to 131 072 points. After this we performed the Fourier transformation (FT) using Python. The spectra are of the reaction at the beginning, middle and end are presented in Fig. 2.

TR-D. We imported the diffusion data using nmrglue and processed each spectrum using a standardized workflow. This included zero-filling (to 131 072 points), phase correction, apodization (0.3 Hz exponential function), and Fourier transformation within the Python environment. After processing, we integrated the region from 5.4 to 7 ppm (as shown in Fig. 2) and stored the resulting values.

We then divided the integrals into overlapping subsets of 32 points acquired over the period of 2 h 14 m, with each subset overlapping the previous one by 31 points, making the time interval between frames equal to 252 s. We used each subset to fit the diffusion coefficient using a mono-exponential decay model:

$$I(G) = Ie^{-D\delta^2\gamma^2G^2(\Delta-\delta/3-\tau/2)} \quad (1)$$

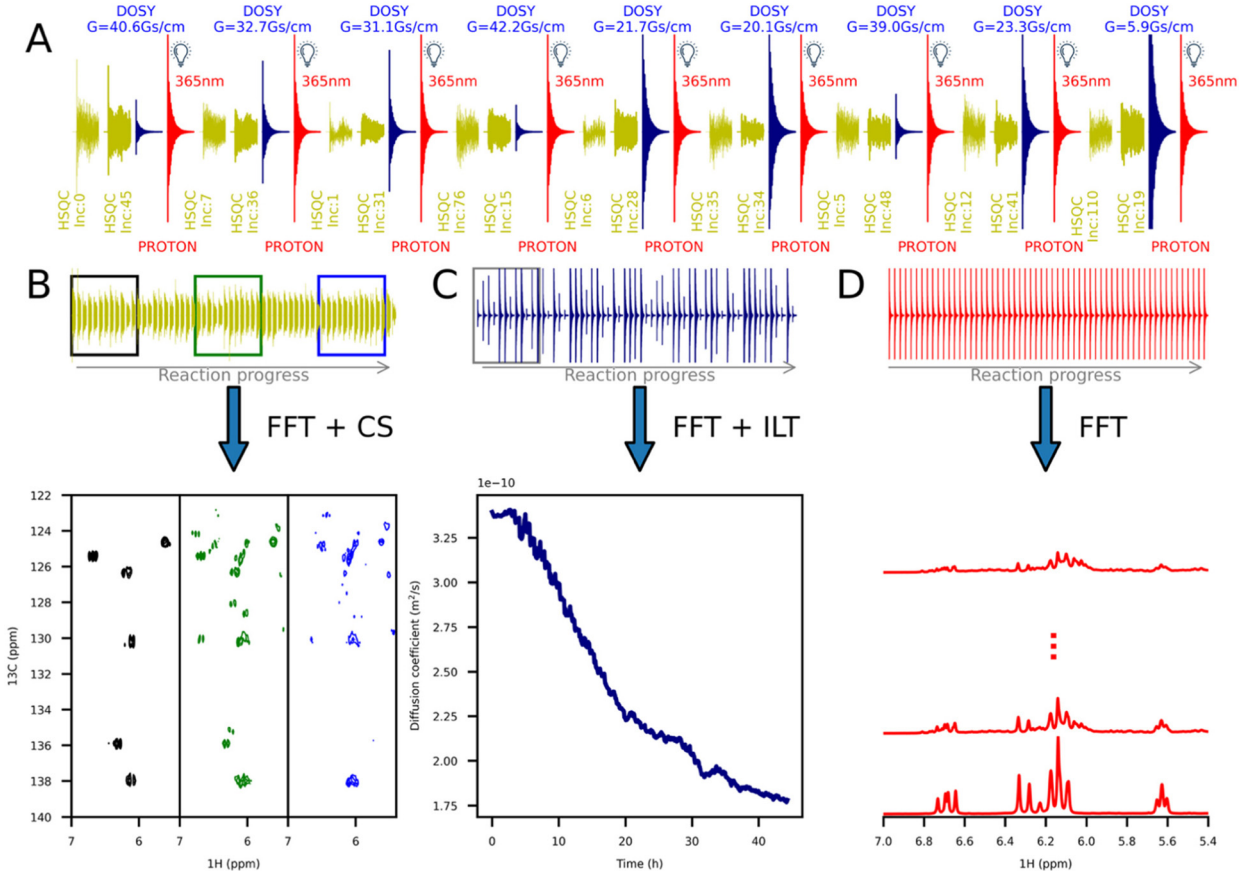

Fig. 1 The representation of the sampling and data processing. (A) illumination of the interleaved acquisition of three different NMR experiments: TR-NUS HSQC (yellow), TR-D (navy), and 1H (red) NMR. Illumination at 365 nm was applied only during the 1H acquisition phase (shown with the symbol of a light-bulb). The sampling scheme for HSQC (increment number for the indirect dimension – inc.) and TR-D (pulsed field gradient – G) is depicted. (B) Moving-frame subsets are extracted from the long NUS acquisition schedule and used as input to a compressed sensing (CS) reconstruction algorithm. The resulting spectra enable continuous visualization and monitoring of the reaction. (C) The TR-D spectra are processed, and the moving-frame subsets are fitted to the Stejskal-Tanner equation to calculate the averaged diffusion coefficient over time. (D) The ^{1}H NMR spectra are processed and analyzed as a fast and rudimentary preview of the changes in the system.

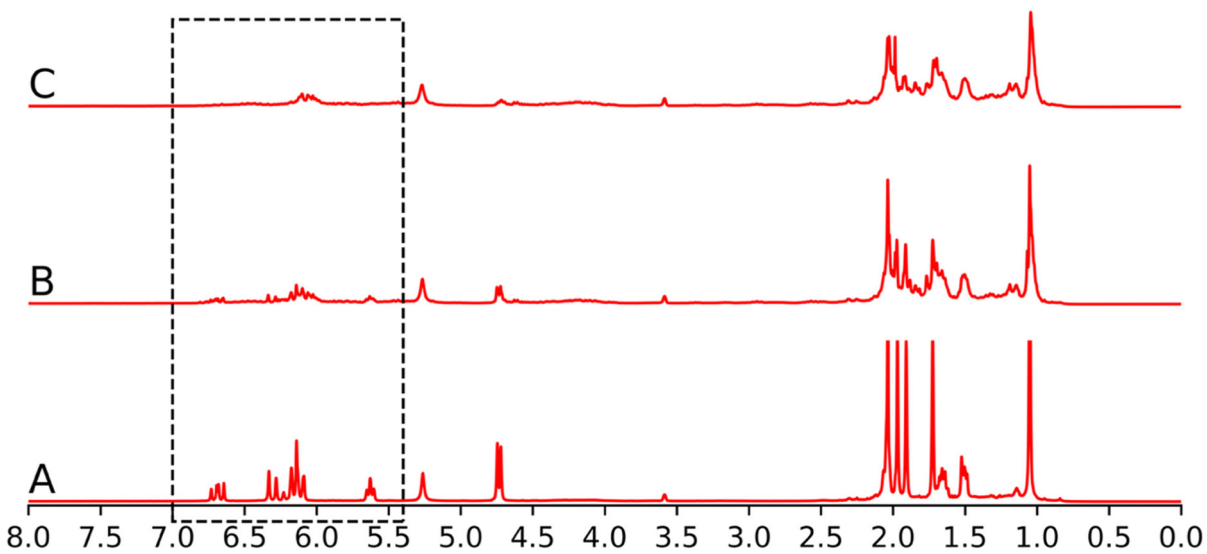

Fig. 2 ^{1}H spectra of the reaction mixture at times: (A) before illumination, (B) at 20 h of illumination, and (C) at the end of the reaction. The highlighted region is the region of the peaks from the polyene chain used in the analysis.

where I is the integral of the peak intensity, G is the pulse field gradient strength, δ is the time of the G, Δ is the diffusion mixing time, τ is a delay between two bipolar pulses, and γ is the gyromagnetic constant of 1H.

In theory, for a small number of overlapping peaks, applying the inverse Laplace transform (ILT) would allow us to resolve the evolution of individual reactants over time. However, ILT analysis was unable to distinguish separate peaks in our data. Therefore, we chose to apply single-exponential fitting only, as shown in Fig. 3.

We converted the diffusion coefficient (D) into molecular mass $\langle M\rangle_D$ using the equation below:[80]

$$D = k(\langle M\rangle_D)^{\alpha} \quad (2)$$

We determined the scaling coefficients k and α empirically by substituting known values of $\langle M\rangle_D$ and of D into eqn (2). We selected reference molecules for this calibration based on their structural symmetry and molecular mass, ensuring similarity to the reactant (RA) and likely photoproducts. We also used the diffusion coefficient from the final subset in the calibration and estimated the corresponding molecular mass by averaging the masses of probable products, weighted by the average intensities of their respective m/z peaks from the mass spectrometry data. The time dependence of such calculated mass ($M_D(t)$) is later used for the assignment of the peaks from TR-NUS HSQC. It is important to stress that this approach can be used only in systems where the viscosity does not change during the reaction. This is usually the case for small molecules. However, in the case of polymers, the change in viscosity can be significant. The problem can be detected by monitoring the diffusion coefficient of a non-reacting molecule.[81] Additionally, the viscosity-independent method for mass determination can be used.[82]

TR-NUS HSQC. To make the workflow as close as possible to the conventional, we have rearranged the TR-NUS data into a series of conventional NUS experiments using a Python script. We set the frame size to 64 points, acquired over the period of 2 h 14 m with a 62-point overlap, making the time interval between frames equal to 252 s. (As we acquired two TR-NUS points for every TR-D point, both of the methods have the same time window.)

Initially, the prepared NUS HSQC spectra were processed in TopSpin. Each spectrum was preprocessed the in the same way: apodization of 1 Hz (exponential function in both dimension) and zero-filled to 4096 (direct dimension) or 256 (indirect dimension). We applied the phase correction parameters from the first spectrum to all subsequent spectra to avoid artifacts from improper phasing. We reconstructed NUS using the Iterative Soft Thresholding Algorithm[83] built in TopSpin. This method was chosen because it is convenient, as it is directly implemented in the spectrometer software. Other algorithms may be used which would give similar results.[84–88] The results of the NUScon competition[89] might be used to choose the method.

Next, we imported the phase-corrected spectra into the kinetics analysis tool Dynamic Centre. As previously mentioned, we saved the integrals of all peaks within the 5.4–7.0 ppm region into a separate spreadsheet. We deconvoluted overlapping peaks by fitting a 2D Lorentzian function using a custom Python script and calculated the peak integrals accordingly. We then smoothed the deconvoluted integrals using the Savitzky–Golay filter to reduce fitting artifacts.

We normalized these peak integrals to a unit value and assigned each peak to a probable photoproduct of the reactant (RA). We summed the signal intensities of all the assigned peaks in the chosen region.

Using this approach, we calculated the average molecular mass of the system over time, denoted as $M_{HSQC}(t)$ using equation:

$$M_{HSQC}(t) = \sum_{reactant} I_{reactant}(t) \times M_{reactant} \quad (3)$$

where, $I_{reactant}(t)$ is the normalized integral of each assigned peak is, and $M_{reactant}$ is its corresponding molecular mass of the molecule assigned to this peak. Due to the limit of the maximum number of experiments analyzed by the Dynamic Centre, we have analyzed the first 35 h of acquisition.

We repeated this analysis for all possible combinations of probable photoproduct assignments to minimize the error between the average mass derived from TR HSQC and that obtained from TR DOSY data. The error (ε) is defined as:

$$\varepsilon = |M_{HSQC}(t) - \langle M\rangle_D(t)| \quad (4)$$

We selected the set of assignments that produced the lowest error for discussion and presented the results in Fig. 4A–C. We show the time dependence of each reactant's peak intensity in Fig. 4D.

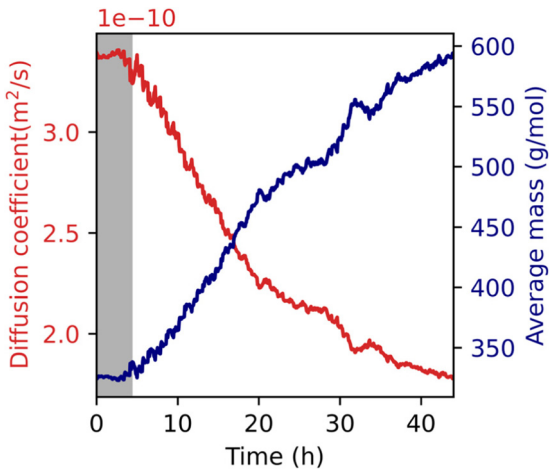

Fig. 3 The average diffusion coefficient and mass change during reaction: the average diffusion coefficient is represented in red, while the average molecular mass is shown in blue. The grayed-out part of the plot represents the beginning of the acquisition without illumination.

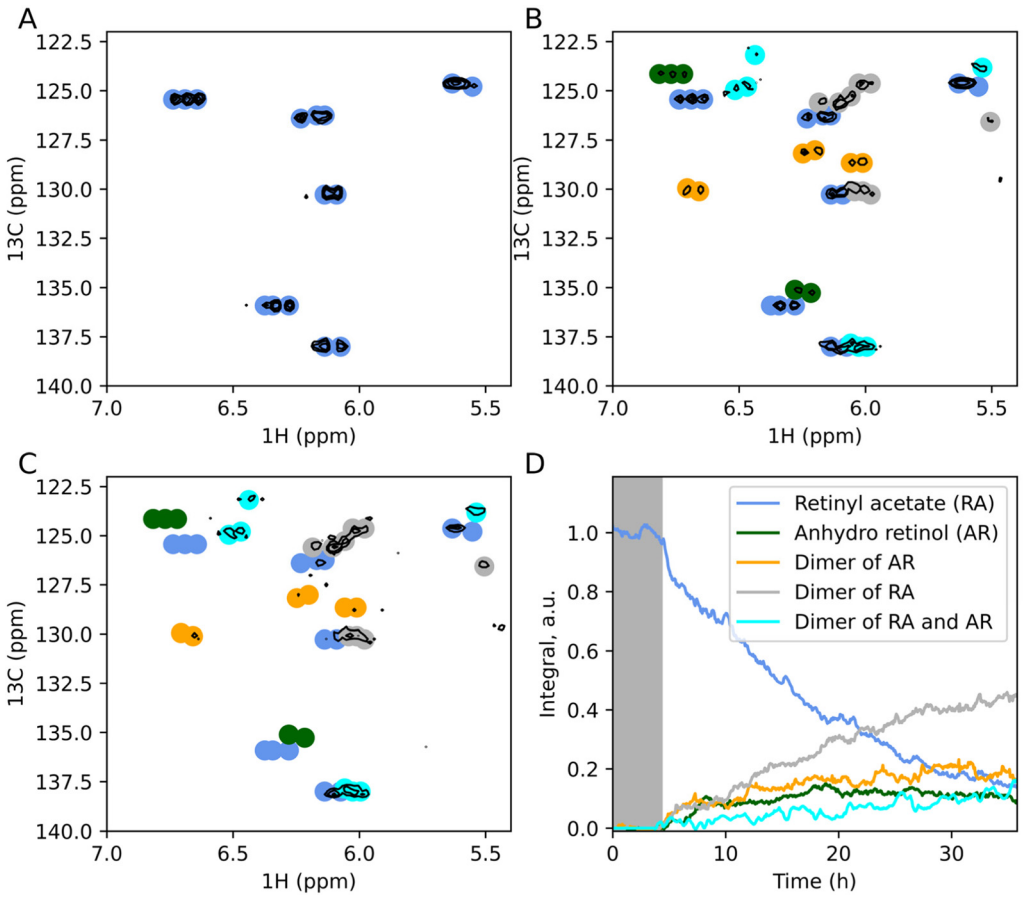

Fig. 4 ^{1}H-^{13}C-HSQC spectra of the reaction: (A–C) HSQC spectra of the reaction mixture at three different time frames: (A) before illumination, (B) after 20 hours of acquisition, and (C) at the end of the reaction. The coloured circles refer to the areas used for integration, with each colour representing the specific monomers and dimers present in the mixture. Cornflower blue represents RA, green represents anhydro retinol (AR), orange represents the homodimer of AR, grey represents the homodimer of RA, and aqua represents the dimer of RA with AR. (D) The integrals of these colored regions shown here illustrate the evolution of products over time. The greyed-out part of the plot represents the beginning of the acquisition without illumination.

Results and discussion

The photodegradation of RA dissolved in deuterated ethanol using 365 nm light was followed by the interleaved acquisition of 3 experiments: ^{1}H NMR, TR-NUS HSQC, and TR-D. The illumination was performed only during the ^{1}H NMR experiment. That illumination scheme was implemented to avoid the influence of the initial heating of the sample when the irradiation level is being changed,[73] which can lead to errors in the diffusion data for the first minutes of acquisition. Our current protocol overcomes this limitation by allowing the system to stabilize during HSQC acquisition before the next TR-D point is acquired. The analysis of the spectra was limited to the region between 5.4 and 7 ppm. This decision was based on two reasons. The first was that the potential products of the reaction found in the literature had peaks in this region from the polyene chain. The other was that this region was free from the signal overlap with the solvent. The acquisition scheme is shown in Fig. 1.

The temporal evolution of the proton spectra shows that new products are being created, and that each spectrum is getting more complex with high overlap (as shown in Fig. 2). This indicates that standard one-dimensional ^{1}H NMR does not provide sufficient information to analyse the studied reaction.

Mass spectrometry

To identify the actual products formed during the photo-illumination study of RA, the reaction mixture was analysed after 46 hours of continuous light exposure using mass spectrometry. The mass spectra were measured as mentioned below. In this study, major photoproducts with m/z values of 268, 536, 596, and 656 were detected as the predominant signals, suggesting the formation of those products upon illumination of RA. These mass values were used as references for peak assignment in the HSQC spectra to assist in the calculation of the average mass of the system.

The analysis of diffusion NMR

The evolution of the average diffusion coefficient of the region (shown in Fig. 3) shows a constant decrease during the reaction time and, by definition, a constant rise of the average mass of the reactants. The change of the mass/diffusion is linear up to ~20 h, and slows down afterwards. This indicates that the photodegradation process leads to the formation of higher-molecular-mass compounds. The possible molecules that might increase the mass are the RA homodimer, AR homodimer, and RA-AR dimer. However, the data itself does not provide a definite answer. The overlapping of many peaks in this region does not allow a viable separation in the diffusion dimension, as even the most powerful inverse Laplace transform algorithms will not be able to differentiate more than 3 overlapping peaks, and even with such a small overlap, they would require a bigger difference of diffusion coefficients.[90–92]

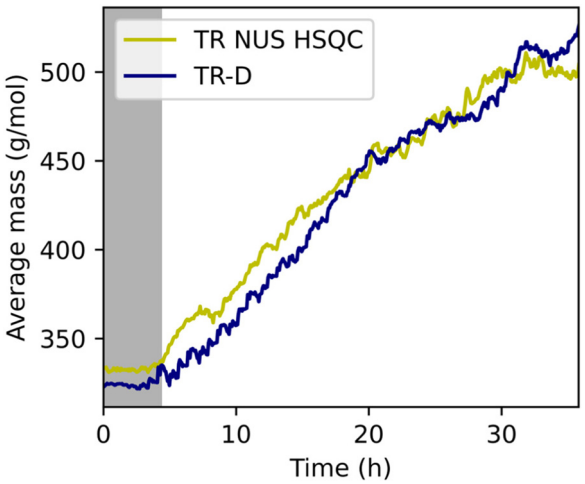

Fig. 5 The average mass evolution calculated from DOSY and HSQC experiments: the time dependence of the average mass is calculated from TR-D (blue) and TR-NUS HSQC (yellow). The grayed-out part of the plot represents the beginning of the acquisition without illumination.

Analysis of TR-NUS HSQC

The first spectra, as recorded before illumination, contained only peaks from retinyl acetate (Fig. 4A). With illumination, more peaks started to appear while the RA was consumed. We have grouped the peaks into four classes with similar time dependence, highlighted with different colours in Fig. 4A–C. The peaks highlighted in cornflower blue obviously correspond to the polyene chain of the RA. The total integral of those peaks is steadily decaying over the course of the illumination. The second group's integral, marked with grey, is constantly rising, similarly, to the aqua-coloured group. The groups highlighted as green and orange are rising only at the beginning of the reaction, while later reaching a plateau. As the number of possible reactants is vast and all the peaks in this region represent similar chemical structures, the traditional assignment strategy of the peaks without any additional information is very challenging. However, some assumptions can be made: *e.g.*, the time-dependence of the integrals of peaks labeled with orange and green suggests that these two intermediates might either undergo further reac-

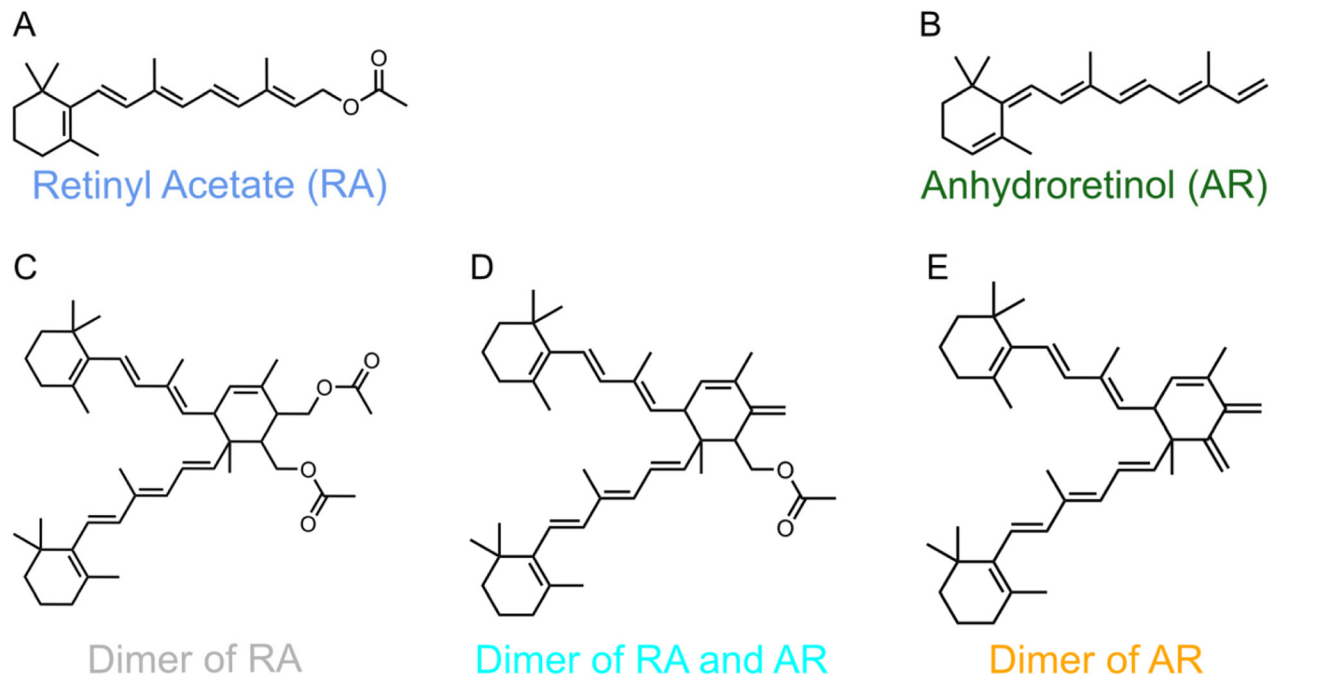

Fig. 6 The structures of possible reactants, (A) retinyl acetate, (B) anhydroretinol, (C) homodimer of RA, (D) heterodimer of RA and AR, (E) homodimer of AR.

tions or be generated only at the beginning of the illumination.

Peak assignment using the synergy of TR-D and TR-NUS

We performed the final assignment using a semi-Monte Carlo approach.[93] From the literature search and mass spectrometry data, we had a list of potential reactants. This list comprises isomers and dimers such as anhydroretinol, β-ionone, retinyl methyl ether, 4-ethoxy anhydroretinol, retinol ethyl ether, the homodimer of retinyl acetate, the dimer of retinyl acetate with anhydroretinol, and the homodimer of anhydroretinol.[26,27,30] Additionally, the result from the mass spectrometry suggests that, in the end, a limited number of dominant species of a particular molar mass occur. The TR-D data allowed us to follow the change of the average mass of the reacting mixture over time. The procedure first required a random assignment of the group of peaks in TR-NUS HSQC to the different molecules and calculation of the average mass evolution $M_{\mathrm{HSQC}}(t)$ using the eqn (3). Then, by calculating the residual between the mass time-dependence from the TR-D and TR-NUS methods (eqn (4)), we found an assignment that was closest to the one from the diffusion analysis. The strategy was similar to the one in our previous work.[73] However, the list of potential reagents was much greater than in that work. We assigned the colour codes in 4D as follows: cornflower blue for RA, green for anhydroretinol (AR), orange for the homodimer of AR, grey for the homodimer of RA, and aqua for the dimer of RA with AR. The resulting average mass evolution calculated from both methods is shown in Fig. 5. The structures of the reactants of this photodecomposition are shown in Fig. 6. It is worth mentioning that the structures of dimers presented in Fig. 6 are only one of the possible ensembles of many isomers, as the dimerization might follow [2 + 2] Diels–Adler or [4 + 2] Diels–Adler reactions. Additionally, as reported previously,[42] the polyene chain of the reactants under the reaction conditions may undergo isomerization.

The temporal profiles of the reactants shown in Fig. 4D are in agreement with a previously reported analysis of this reaction and can be explained by a two-stage photoreaction, where in the first stage, the RA forms AR, and in the second stage, the three products form dimers. Additionally, this assignment is supported by the mass spectroscopy data. Moreover, it is worth mentioning that, as shown by our previous work,[73] that the method is very robust to the noise and the limit of detection is set by the HSQC.

Conclusions

We have analysed the process of photodegradation of retinyl acetate in ethanol using an *in situ* NMR approach with interleaved TR-NUS HSQC and TR-D methods. The approach allowed for the study of the temporal profile of a complex reaction with many possible pathways, which were described in the literature. The description of the final reaction is in agreement with previous studies, and it is additionally confirmed by the mass spectroscopy data. This shows that the utilization of interleaved TR-NUS and TR-D NMR spectroscopy is highly valuable in the analysis of complex reactions with multiple possible products and intermediates, even with similar structures, which can make the conventional assignment close to impossible. Based on the assignment and time-dependence, we propose the simple reaction pathways in which the RA follows two pathways: dimerization and degradation into AR. Both RA and AR also follow both homo- and hetero-dimerization, forming three dimers. However, as discussed, the dimers reported in this work are not the only possible structures in the reaction; most likely, they form an ensemble of different isomers.

However, the reader has to be aware that the method itself is based on the change in the molecular mass and therefore will only work for systems where a significant change in the mass occurs. In a situation of structural change that will not affect the diffusion coefficients of the molecule, that approach will be invalid.

The method can be additionally extended for the combined NMR UV-VIS setup.[94–96] Information from UV-Vis may be used to track the evolution of absorption at the excitation wavelength over time, enabling full kinetic modelling of the system.

Author contributions

FK: formal analysis, investigation, methodology, software, validation, visualization, writing – original draft; CMG: conceptualization, formal analysis, investigation, methodology, software, supervision, validation, visualization, writing – original draft; FFW: conceptualization, methodology, software; LM: investigation; RMG: conceptualization, funding acquisition; TR: conceptualization, writing – original draft; MU: conceptualization, data curation, funding acquisition, investigation, methodology, project administration, resources, software, supervision, validation, visualization, writing – review & editing.

Conflicts of interest

There are no conflicts to declare.

Data availability

The raw data, processing scripts, and processed data used in the work and figure preparation are available at: https://doi.org/10.18150/XA0VUQ

The scripts to set up the acquisition and to control illumination are available at: https://github.com/murbanczyk/insitu_photoNMR_trD_trNUS

Supplementary information (SI): mass spectrometry data, list of molecules with their molecular mass and diffusion

coefficient-mass calibration data. See DOI: https://doi.org/10.1039/d6an00072j.

Acknowledgements

FK, MGC, and MU acknowledge financial support from the National Science Centre, Poland, in the form of a grant SONATA (project no. 2022/47/D/ST4/00846).

FFW wants to thank the Institute of Physical Chemistry, PAS, and its members for their hospitality.

FFW and RMG would like to thank the Deutsche Forschungsgemeinschaft for funding (DFG, RTG 2620 IonPairs in Reaction Project 426795949).

References

1 E. G. Moschetta, G. C. Cook, L. J. Edwards, M. A. Ischay, Z. Lei, F. Buono, F. Lévesque, J. A. O. Garber, M. MacTaggart, M. Sezen-Edmonds, K. P. Cole, M. G. Beaver, J. Doerfler, S. M. Opalka, W. Liang, P. D. Morse and N. Miyake, *Org. Process Res. Dev.*, 2024, **28**, 831–846.

2 B. D. Fairbanks, L. J. Macdougall, S. Mavila, J. Sinha, B. E. Kirkpatrick, K. S. Anseth and C. N. Bowman, *Chem. Rev.*, 2021, **121**, 6915–6990.

3 D. Cambié, C. Bottecchia, N. J. W. Straathof, V. Hessel and T. Noël, *Chem. Rev.*, 2016, **116**, 10276–10341.

4 D. Vione, M. Minella, V. Maurino and C. Minero, *Chem. – Eur. J.*, 2014, **20**, 10590–10606.

5 S. Saha and J. F. Stoddart, *Chem. Soc. Rev.*, 2007, **36**, 77–92.

6 A. W. Hains, Z. Liang, M. A. Woodhouse and B. A. Gregg, *Chem. Rev.*, 2010, **110**, 6689–6735.

7 A. H. Gelebart, D. Jan Mulder, M. Varga, A. Konya, G. Vantomme, E. W. Meijer, R. L. B. Selinger and D. J. Broer, *Nature*, 2017, **546**, 632–636.

8 S. Dong, A. Ong and C. Chi, *J. Photochem. Photobiol., C*, 2019, **38**, 27–46.

9 A. Mames, A. Gorski, J. Jankowska, T. Ratajczyk and M. Pietrzak, *Phys. Chem. Chem. Phys.*, 2024, **26**, 28171–28181.

10 A. K. Haritash and C. P. Kaushik, *J. Hazard. Mater.*, 2009, **169**, 1–15.

11 K. Wang, Y. Kou, K. Wang, C. Guo, X. Liang, M. Wang, J. Li, S. Liang, W. Wang and J. Wang, *Sep. Purif. Technol.*, 2025, **376**, 134041.

12 C. B. Stephensen, *Annu. Rev. Nutr.*, 2001, **21**, 167–192.

13 J. Reichrath, B. Lehmann, C. Carlberg, J. Varani and C. C. Zouboulis, *Horm. Metab. Res.*, 2007, **39**, 71–84.

14 W. Bonrath, B. Gao, P. Houston, T. McClymont, M. A. Müller, C. Schäfer, C. Schweiggert, J. Schütz and J. A. Medlock, *Org. Process Res. Dev.*, 2023, **27**, 1557–1584.

15 R. C. Moon, C. J. Grubbs, M. B. Sporn and D. G. Goodman, *Nature*, 1977, **267**, 620–621.

16 H. Yin, Y. Liu, S. Yuan and Z. Chen, *Food Sci. Technol. Res.*, 2014, **20**, 841–847.

17 S. M. Loveday and H. Singh, *Trends Food Sci. Technol.*, 2008, **19**, 657–668.

18 R. Blomhoff and H. K. Blomhoff, *J. Neurobiol.*, 2006, **66**, 606–630.

19 E. M. Olsen, J. D. Harvey, D. C. Hill and H. D. Branion, *Poult. Sci.*, 1959, **38**, 929–942.

20 H. E. Chen, H. Y. Peng and B. H. Chen, *Food Chem.*, 1996, **57**, 497–503.

21 R. M. D. Fávaro, M. H. Iha, T. C. Mazzi, R. Fávaro and M. D. L. P. Bianchi, *Food Chem.*, 2011, **126**, 827–830.

22 M. S. Butt, M. U. Arshad, M. S. Alam and M. T. Nadeem, *Food Res. Int.*, 2007, **40**, 1212–1219.

23 A. A. AlBahrani, V. Rotarou, P. J. Roche and R. F. Greaves, *Clin. Chem. Lab. Med.*, 2016, **54**, 1609–1618.

24 C. Cuerq, N. Peretti, K. Chikh, A. Mialon, M. Guillaumont, J. Drai and E. Blond, *Ann. Clin. Biochem.*, 2015, **52**, 259–269.

25 T. Karakosta, Y. Wan and D. Truong, *Clin. Biochem.*, 2023, **115**, 144–148.

26 P. P. Fu, S. H. Cheng, L. Coop, Q. Xia, S. J. Culp, W. H. Tolleson, W. G. Wamer and P. C. Howard, *J. Environ. Sci. Health, Part C:Environ. Carcinog. Ecotoxicol. Rev.*, 2003, **21**, 165–197.

27 W. H. Tolleson, S.-H. Cherng, Q. Xia, M. Boudreau, J. J. Yin, W. G. Wamer, P. C. Howard, H. Yu and P. P. Fu, *Int. J. Environ. Res. Public Health*, 2005, **2**, 147–155.

28 P. P. Fu, Q. Xia, J. J. Yin, S.-H. Cherng, J. Yan, N. Mei, T. Chen, M. D. Boudreau, P. C. Howard and W. G. Wamer, *Photochem. Photobiol.*, 2007, **83**, 409–424.

29 G. M. Landers and J. A. Olson, *J. Assoc. Off. Anal. Chem.*, 1986, **69**, 50–55.

30 M. Mousseron-Canet, *Methods Enzymol.*, 1971, **18**, 591–615.

31 Y. Takashima, T. Nakajima, S. Tanaka, M. Washitake, T. Anmo and H. Matsumaru, *Chem. Pharm. Bull.*, 1979, **27**, 1553–1563.

32 T. Rosenfeld, A. Alchalal and M. Ottolenghi, *Chem. Phys. Lett.*, 1973, **20**, 291–297.

33 B. S. Sherman, *Clin. Chem.*, 1967, **13**, 1039–1049.

34 Y. Mase, *J. Vitaminol.*, 1962, **8**, 15–19.

35 P. F. Corey, H. Arndt, J. P. Albarella, A. M. Reddy and V. J. Rao, *J. Org. Chem.*, 1992, **57**, 6727–6731.

36 G. Paquette and M. A. Kanaan, *Food Chem.*, 1985, **18**, 211–231.

37 P. E. Blatz and D. L. Pippert, *J. Am. Chem. Soc.*, 1968, **90**, 1296–1300.

38 S. H. Cherng, Q. Xia, L. R. Blankenship, J. P. Freeman, W. G. Wamer, P. C. Howard and P. P. Fu, *Chem. Res. Toxicol.*, 2005, **18**, 129–138.

39 Q. Xia, J. J. Yin, W. G. Wamer, S. H. Cherng, M. D. Boudreau, P. C. Howard, H. Yu and P. P. Fu, *Int. J. Environ. Res. Public Health*, 2006, **3**, 185–190.

40 C. D. Robeson, T. D. Cawley, L. Weisler, M. H. Stern, C. C. Eddinger and A. J. Chechak, *J. Am. Chem. Soc.*, 1955, **77**, 4111–4119.

41 S. Isoe, S. B. Hyeon, S. Katsumura and T. Sakan, *Tetrahedron Lett.*, 1972, **13**, 2517–2520.
42 S. Zhang, H. Yin, S. Yuan, Z. Chen and Q. Zhang, *ACS Food Sci. Technol.*, 2025, **5**, 1990–1998.
43 M. Khajeh, M. A. Bernstein and G. A. Morris, *Magn. Reson. Chem.*, 2010, **48**, 516–522.
44 D. A. Foley, E. Bez, A. Codina, K. L. Colson, M. Fey, R. Krull, D. Piroli, M. T. Zell and B. L. Marquez, *Anal. Chem.*, 2014, **86**, 12008–12013.
45 M. Pietrzak, J. Dobkowski, A. Gorski, S. Gawinkowski, M. Kijak, R. Luboradzki, P. E. Hansen and J. Waluk, *Phys. Chem. Chem. Phys.*, 2014, **16**, 9128–9137.
46 L. Buljubasich, B. Blümich and S. Stapf, *Chem. Eng. Sci.*, 2010, **65**, 1394–1399.
47 F. Dalitz, M. Cudaj, M. Maiwald and G. Guthausen, *Prog. Nucl. Magn. Reson. Spectrosc.*, 2012, **60**, 52–70.
48 D. Gołowicz, K. Kazimierczuk, M. Urbańczyk and T. Ratajczyk, *ChemistryOpen*, 2019, **8**, 196–200.
49 M. Leutzsch, A. J. Sederman, L. F. Gladden and M. D. Mantle, *Magn. Reson. Imaging*, 2019, **56**, 138–143.
50 C. Jacquemmoz, F. Giraud and J. N. Dumez, *Analyst*, 2020, **145**, 478–485.
51 K. Zangger, *Prog. Nucl. Magn. Reson. Spectrosc.*, 2015, **86–87**, 1–20.
52 C. S. Johnson Jr, *Prog. Nucl. Magn. Reson. Spectrosc.*, 1999, **34**, 203–256.
53 A. B. Jones, G. C. Lloyd-Jones and D. Uhrín, *Anal. Chem.*, 2017, **89**, 10013–10021.
54 A. Shchukina, M. Kaźmierczak, P. Kasprzak, M. Davy, G. R. Akien, C. P. Butts and K. Kazimierczuk, *Chem. Commun.*, 2019, **55**, 9563–9566.
55 H. Zhan, Y. Ni, L. Zhou, L. Ji, J. Liu, Y. Yang, Y. Huang and Z. Chen, *Cell Rep. Phys. Sci.*, 2025, **6**, 102863.
56 H. Zhan, J. Liu, Q. Fang, X. Chen and L. Hu, *Anal. Chem.*, 2024, **96**, 1515–1521.
57 Y. Shrot and L. Frydman, *J. Magn. Reson.*, 2008, **195**, 226–231.
58 V. V. Telkki, M. Urbańczyk and V. Zhivonitko, *Prog. Nucl. Magn. Reson. Spectrosc.*, 2021, **126–127**, 101–120.
59 L. H. K. Queiroz, P. Giraudeau, F. A. B. Dos Santos, K. T. De Oliveira and A. G. Ferreira, *Magn. Reson. Chem.*, 2012, **50**, 496–501.
60 M. Urbańczyk, A. Shchukina, D. Gołowicz and K. Kazimierczuk, *Magn. Reson. Chem.*, 2019, **57**, 4–12.
61 M. Mayzel, J. Rosenlöw, L. Isaksson and V. Y. Orekhov, *J. Biomol. NMR*, 2014, **58**, 129–139.
62 D. Gołowicz, P. Kasprzak, V. Orekhov and K. Kazimierczuk, *Prog. Nucl. Magn. Reson. Spectrosc.*, 2020, **116**, 40–55.
63 L. Frydman, T. Scherf and A. Lupulescu, *Proc. Natl. Acad. Sci. U. S. A.*, 2002, **99**, 15858–15862.
64 G. Hamdoun, L. Guduff, C. Van Heijenoort, C. Bour, V. Gandon and J. N. Dumez, *Analyst*, 2018, **143**, 3458–3464.
65 B. Gouilleux, B. Charrier, E. Danieli, J. N. Dumez, S. Akoka, F. X. Felpin, M. Rodriguez-Zubiri and P. Giraudeau, *Analyst*, 2015, **140**, 7854–7858.
66 P. Giraudeau and L. Frydman, *Annu. Rev. Anal. Chem.*, 2014, **7**, 129–161.
67 R. Dass, W. Kozminski and K. Kazimierczuk, *Anal. Chem.*, 2015, **87**, 1337–1343.
68 D. Gołowicz, M. Kaźmierczak and K. Kazimierczuk, *Magn. Reson. Chem.*, 2021, **59**, 213–220.
69 M. Urbańczyk, D. Bernin, A. Czuroń and K. Kazimierczuk, *Analyst*, 2016, **141**, 1745–1752.
70 T. S. C. MacDonald, W. S. Price and J. E. Beves, *ChemPhysChem*, 2019, **20**, 926–930.
71 L. L. Fillbrook, M. D. Nothling, M. H. Stenzel, W. S. Price and J. E. Beves, *ACS Macro Lett.*, 2022, **11**, 166–172.
72 M. Urbańczyk, Y. Kharbanda, O. Mankinen and V. V. Telkki, *Anal. Chem.*, 2020, **92**, 9948–9955.
73 K. Kristinaityte, A. Mames, M. Pietrzak, F. F. Westermair, W. Silva, R. M. Gschwind, T. Ratajczyk and M. Urbańczyk, *J. Am. Chem. Soc.*, 2022, **144**, 13938–13945.
74 C. Feldmeier, H. Bartling, E. Riedle and R. M. Gschwind, *J. Magn. Reson.*, 2013, **232**, 39–44.
75 V. Yu. Orekhov, V. Jaravine, M. Mayzel and K. Kazimierczuk, MddNMR - Reconstruction of NMR spectra from NUS signal using MDD and CS, https://mddnmr.spektrino.com.
76 J. J. Helmus and C. P. Jaroniec, *J. Biomol. NMR*, 2013, **55**, 355–367.
77 C. R. Harris, K. J. Millman, S. J. van der Walt, R. Gommers, P. Virtanen, D. Cournapeau, E. Wieser, J. Taylor, S. Berg, N. J. Smith, R. Kern, M. Picus, S. Hoyer, M. H. van Kerkwijk, M. Brett, A. Haldane, J. F. del Río, M. Wiebe, P. Peterson, P. Gérard-Marchant, K. Sheppard, T. Reddy, W. Weckesser, H. Abbasi, C. Gohlke and T. E. Oliphant, *Nature*, 2020, **585**(7825), 357–362.
78 P. Virtanen, R. Gommers, T. E. Oliphant, M. Haberland, T. Reddy, D. Cournapeau, E. Burovski, P. Peterson, W. Weckesser, J. Bright, S. J. van der Walt, M. Brett, J. Wilson, K. J. Millman, N. Mayorov, A. R. J. Nelson, E. Jones, R. Kern, E. Larson, C. J. Carey, İ. Polat, Y. Feng, E. W. Moore, J. VanderPlas, D. Laxalde, J. Perktold, R. Cimrman, I. Henriksen, E. A. Quintero, C. R. Harris, A. M. Archibald, A. H. Ribeiro, F. Pedregosa, P. van Mulbregt, A. Vijaykumar, A. Pietro Bardelli, A. Rothberg, A. Hilboll, A. Kloeckner, A. Scopatz, A. Lee, A. Rokem, C. N. Woods, C. Fulton, C. Masson, C. Häggström, C. Fitzgerald, D. A. Nicholson, D. R. Hagen, D. V. Pasechnik, E. Olivetti, E. Martin, E. Wieser, F. Silva, F. Lenders, F. Wilhelm, G. Young, G. A. Price, G. L. Ingold, G. E. Allen, G. R. Lee, H. Audren, I. Probst, J. P. Dietrich, J. Silterra, J. T. Webber, J. Slavič, J. Nothman, J. Buchner, J. Kulick, J. L. Schönberger, J. V. de Miranda Cardoso, J. Reimer, J. Harrington, J. L. C. Rodríguez, J. Nunez-Iglesias, J. Kuczynski, K. Tritz, M. Thoma, M. Newville, M. Kümmerer, M. Bolingbroke, M. Tartre, M. Pak, N. J. Smith, N. Nowaczyk, N. Shebanov, O. Pavlyk, P. A. Brodtkorb, P. Lee, R. T. McGibbon, R. Feldbauer, S. Lewis, S. Tygier, S. Sievert, S. Vigna, S. Peterson, S. More, T. Pudlik, T. Oshima, T. J. Pingel, T. P. Robitaille, T. Spura, T. R. Jones, T. Cera, T. Leslie, T. Zito, T. Krauss,

U. Upadhyay, Y. O. Halchenko and Y. Vázquez-Baeza, *Nat. Methods*, 2020, **17**(3), 261–272.
79 J. D. Hunter, *Comput. Sci. Eng.*, 2007, **9**, 90–95.
80 R. Raghavan, T. L. Maver and F. D. Blum, *Macromolecules*, 1987, **20**, 814–818.
81 M. Czarnota, M. Cybularczyk-Cecotka, F. F. Westermair, F. A. Campos, K. Kapil, K. Matyjaszewski, G. Szczepaniak and M. Urbańczyk, *Polym. Chem.*, 2026, **17**, 1109–1115.
82 F. Arrabal-Campos, P. Ona-Burgos and I. Fernandez, *Polym. Chem.*, 2016, **7**, 4326–4329.
83 K. Kazimierczuk and V. Y. Orekhov, *Angew. Chem., Int. Ed.*, 2011, **50**, 5556–5559.
84 S. G. Hyberts, A. G. Milbradt, A. B. Wagner, H. Arthanari and G. Wagner, *J. Biomol. NMR*, 2012, **52**, 315–327.
85 G. Karunanithy and D. F. Hansen, *J. Biomol. NMR*, 2021, **75**, 179–191.
86 A. Jahangiri, X. Han, D. Lesovoy, T. Agback, P. Agback, A. Achour and V. Orekhov, *J. Magn. Reson.*, 2023, **346**, 107342.
87 X. Qu, Y. Huang, H. Lu, T. Qiu, D. Guo, T. Agback, V. Orekhov, Z. Chen, X. Qu, Y. Huang, H. Lu, T. Qiu, Z. Chen, D. Guo, T. Agback and V. Orekhov, *Angew. Chem., Int. Ed.*, 2020, **59**, 10297–10300.
88 X. Qu, M. Mayzel, J.-F. Cai, Z. Chen and V. Orekhov, *Angew. Chem., Int. Ed.*, 2015, **54**, 852–854.
89 Y. Pustovalova, F. Delaglio, D. L. Craft, H. Arthanari, A. Bax, M. Billeter, M. J. Bostock, H. Dashti, D. F. Hansen, S. G. Hyberts, B. A. Johnson, K. Kazimierczuk, H. Lu, M. Maciejewski, T. M. Miljenović, M. Mobli, D. Nietlispach, V. Orekhov, R. Powers, X. Qu, S. A. Robson, D. Rovnyak, G. Wagner, J. Ying, M. Zambrello, J. C. Hoch, D. L. Donoho and A. D. Schuyler, *Magn. Reson.*, 2021, **2**, 843–861.
90 M. Urbańczyk, D. Bernin, W. Koźmiński and K. Kazimierczuk, *Anal. Chem.*, 2013, **85**, 1828–1833.
91 K. Xu and S. Zhang, *Anal. Chem.*, 2014, **86**, 592–599.
92 A. Cherni, E. Chouzenoux and M.-A. Delsuc, *Analyst*, 2016, **142**, 772–779.
93 N. Metropolis and S. Ulam, *J. Am. Stat. Assoc.*, 1949, **44**, 335.
94 D. Herold, M. Brauser, J. Kind and C. M. Thiele, *Chem. – Eur. J.*, 2024, **30**, e202304016.
95 A. Seegerer, P. Nitschke and R. M. Gschwind, *Angew. Chem., Int. Ed.*, 2018, **57**, 7493–7497.
96 P. M. Tolstoy, B. Koeppe, G. S. Denisov and H. H. Limbach, *Angew. Chem., Int. Ed.*, 2009, **48**, 5745–5747.